Analytical Dispersion Analysis of Loaded Periodic Circuits Using the Generalized Scattering Matrix

W. Scott Best, *Member, IEEE*, Ronald J. Riegert, and Lewis C. Goodrich

***Abstract*—The dispersion characteristics of periodic circuits are typically determined analytically using idealized circuit models. Idealized circuit models exclude the effects that circuit asymmetries, such as those created by coupling ports, have on accurately determining the system normal mode dispersion characteristics for physically loaded periodic circuits. A new analytical dispersion analysis technique has been developed to accurately predict the dispersion characteristics for loaded periodic circuits. The loaded periodic circuit dispersion analysis problem is resolved using the frequency dependent mode matching algorithm, which yields regional normal mode scattering information for the circuit in the form of the generalized scattering matrix (GSM). The GSM is manipulated to determine the normal mode amplitudes for each region of the periodic circuit, where the resulting regional normal mode amplitude information is used to construct electromagnetic field maps for the length of the periodic circuit. Spatial Fourier analysis of a frequency-dependent field map determines the periodicity of the spatially dependent field. The resulting frequency-dependent spatial Fourier harmonic information is used to construct three-dimensional (3-D) and two-dimensional (2-D) system normal mode dispersion diagrams for loaded periodic circuits. The 2-D and 3-D dispersion diagrams define the phase, frequency, and relative amplitude characteristics of the periodic circuit system normal modes excited by the coupling ports. The system normal mode amplitude information defines the relative level of excitation for a given mode in comparison to other modes on the dispersion diagram.**

I. Introduction

THE SYSTEM normal mode dispersion characteristics of periodic circuits are typically determined using idealized models of the circuit [1]–[3]. Idealized models of periodic circuits ignore the effects of coupling ports on the system normal mode dispersion characteristics. Coupling ports interrupt the periodicity of the circuit, causing field asymmetries in the regions of the circuit local to the coupling ports. The field asymmetries lead to frequency and phase shifts of the loaded system normal mode dispersion characteristics from the idealized system normal mode dispersion characteristics. The perturbed system normal mode dispersion characteristics of a finite length loaded periodic circuit are typically determined by building a prototype of the circuit and measuring the dispersion characteristics of the circuit [4]. The experimental data is then used to iteratively modify the design of the hardware from which the loaded periodic circuit is constructed to obtain the desired dispersion characteristics. This approach results in an empirical design for the hardware.

Manuscript received June 16, 1995; revised August 26, 1996.

The authors are with DuPont Central Research and Development, Wilmington, DE 19880-0357 USA.

Publisher Item Identifier S 0018-9480(96)08481-5.

A novel experimental technique to accurately measure the system normal mode dispersion characteristics of finite length loaded periodic circuits was previously developed and demonstrated [2], [5]. The experimental technique uses miniature minimally perturbing monopole antennas to spatially map the frequency dependent vector electromagnetic fields for the circuit. The resulting field maps are Fourier analyzed to determine the periodicity of the frequency dependent spatial field maps. The frequency dependent Fourier harmonic information for the circuit being analyzed is used to construct two-dimensional (2-D) and three-dimensional (3-D) system normal mode dispersion diagrams. This experimental technique yields accurate system normal mode dispersion diagrams for measured circuits, but at the expense of constructing the hardware to determine the dispersion characteristics. This technique is still time consuming, costly, and is prone to error if the miniature monopole antennas are not designed to minimize field perturbations.

A new loaded finite length periodic circuit system normal mode dispersion design algorithm, however, has been developed using an analytical field mapping technique to calculate the complex vector electromagnetic vector fields for any discretized location in a waveguide assembly forming a periodic circuit. This is accomplished using the mode-matching algorithm [2], [6], [7], [8]. Frequency-dependent spatial electromagnetic field maps are obtained analytically by manipulating the generalized scattering matrix (GSM) determined from the mode matching algorithm to solve for the regional normal mode amplitudes. The accuracy of the complex electromagnetic field maps is dependent on the sum of the normal modes used to model each region of the loaded periodic circuit. The accuracy or convergence of the solution is defined as the relative convergence (RC) criterion [2], [6], [9], [10] for the mode matching algorithm. The resulting frequency dependent spatial field maps are Fourier analyzed, from which the 3-D and 2-D system normal mode dispersion diagrams for the loaded circuit are created.

This analytic design tool for determining the dispersion characteristics of a loaded finite length periodic circuit eliminates the necessity of constructing hardware to measure the dispersion characteristics of the circuit. The information is obtained analytically, which reduces the design and construction time for loaded periodic circuits and eliminates costly dispersion design errors. Section II introduces the analytical dispersion analysis algorithms developed using the GSM for idealized infinitely periodic circuits, and for loaded finite length period circuits. Section III presents a comparison

0018–9480/96$05.00 © 1996 IEEE

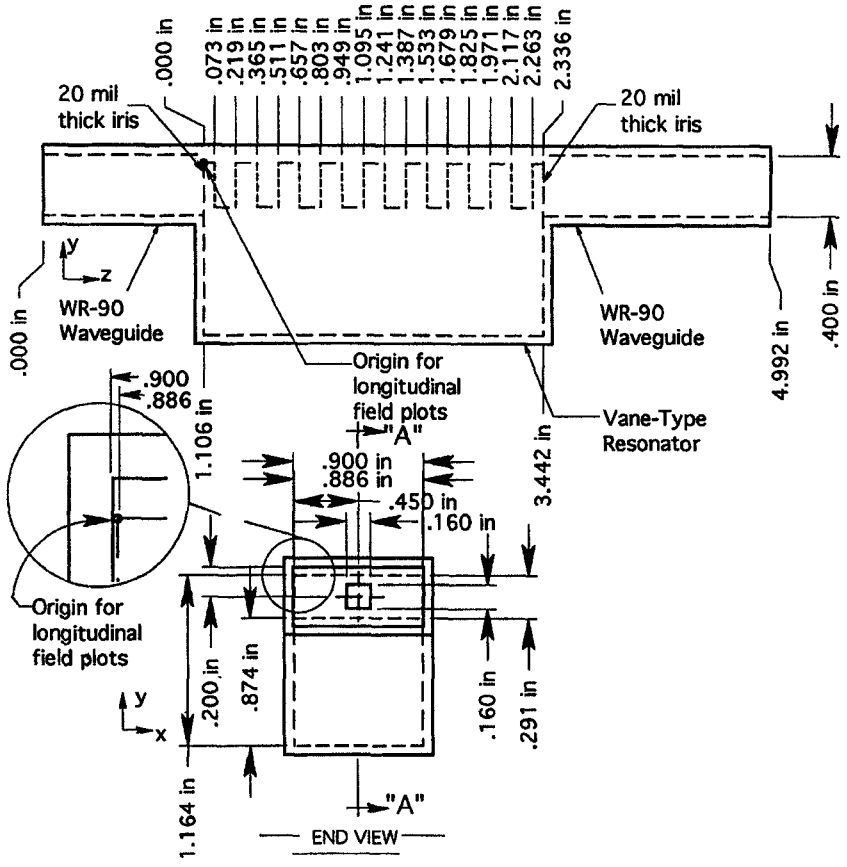

Fig. 1. Eight-period loaded finite length vane-type waveguide resonator configuration.

between the idealized dispersion model and the loaded finite length dispersion model for a highly overmoded eight-period vane-type waveguide resonator. Section IV concludes and summarizes this effort.

II. Analytical Dispersion Analysis Using the GSM

The GSM determined using the mode matching algorithm provides a generalized analytical tool for determining the system normal mode dispersion characteristics for both idealized infinitely periodic circuits [1]–[3] and for finite length loaded period circuits [2], [5]. These two dispersion analysis methods form complementary tools, where the idealized infinitely periodic circuit dispersion model for a single period of the circuit is used to design the prototype circuit configuration, and the finite length loaded periodic circuit dispersion modeling technique is used to design coupling ports for the loaded periodic circuit to optimally excite specific system normal modes.

The two GSM dispersion analysis algorithms are demonstrated using the eight-period linear vane-type waveguide resonator shown in Figs. 1 and 2. The analysis process begins by determining the system normal mode dispersion characteristics for a single period of the eight period circuit using the idealized circuit model [2], [3]. The circuit shown in Figs. 1 and 2 is then analyzed to determine the dispersion characteristics of the system normal modes excited by the two coupling ports.

The GSM for a single period of the vane-type waveguide circuit shown in Figs. 1 and 2 is represented in terms of the regional normal mode scattering variables $(\vec{a}_1, \vec{b}_1, \vec{a}_2, \vec{b}_2)$ as

$$\begin{bmatrix} \overline{\overline{S_{11}}} & \overline{\overline{S_{12}}} \\ \overline{\overline{S_{21}}} & \overline{\overline{S_{22}}} \end{bmatrix} \begin{bmatrix} \vec{a}_1 \\ \vec{a}_2 \end{bmatrix} = \begin{bmatrix} \vec{b}_1 \\ \vec{b}_2 \end{bmatrix}. \tag{1}$$

Floquet's theorem [1] permits (1) to be manipulated into the form of a Generalized Eigenvalue Equation [2], [3]

$$\begin{bmatrix} \bar{\bar{1}} - \overline{\overline{S_{22}S_{11}}} & -\overline{\overline{S_{22}S_{12}}} \\ \overline{\overline{S_{11}}} & \overline{\overline{S_{12}}} \end{bmatrix} \begin{bmatrix} \vec{a}_1 \\ \vec{a}_2 \end{bmatrix} = \begin{bmatrix} \overline{\overline{S_{21}e^{-\Gamma_n L}}} & \bar{\bar{0}} \\ \bar{\bar{0}} & \overline{\overline{e^{-\Gamma_n L}}} \end{bmatrix} \begin{bmatrix} \vec{a}_1 \\ \vec{a}_2 \end{bmatrix} \tag{2}$$

where the eigenvalues define the system normal mode propagation constants, $\Gamma_n = \alpha_n + j\beta_n$. Equation (2) has been previously used to analyze the system normal mode dispersion characteristics for a single period of the circuit shown in Figs. 1 and 2 [2], [3]. The idealized system normal mode dispersion characteristics are shown in Fig. 3 in comparison to experimental dispersion data determined using the resonance technique [4] for the eight-period linear vane-type waveguide resonator.

In general, the idealized dispersion analysis performed with (2) is potentially in error due to the field asymmetries introduced to the periodic circuit by the interruption of the circuit periodicity with the coupling ports shown in Figs. 1 and 2. The resulting field asymmetries can perturb the frequency and phase response of the idealized system normal mode dispersion characteristics shown in Fig. 3. Coupling ports can also mutually excite multiple system normal modes. The

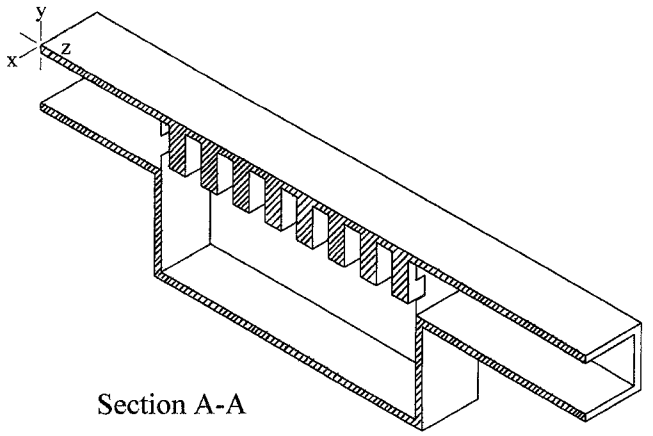

Fig. 2. Isometric view of the eight-period loaded finite length linear vane-type waveguide resonator shown in Fig. 1.

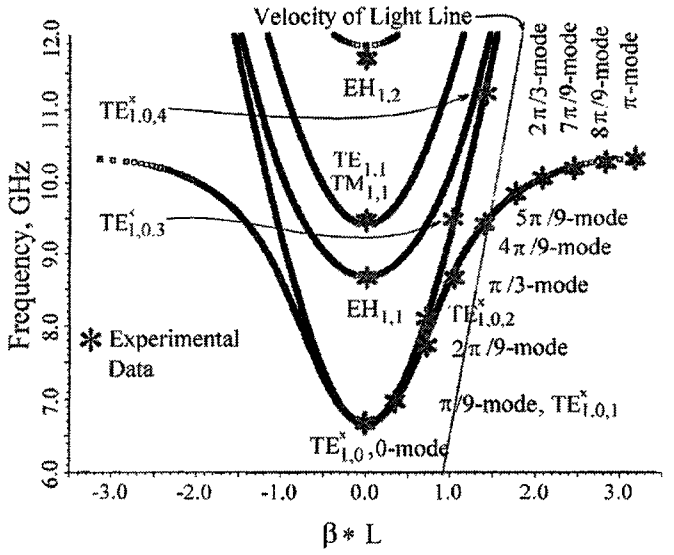

Fig. 3. Idealized GSM dispersion diagram determined for the first passband of the linear vane-type waveguide shown in Fig. 1.

ability to analytically determine the loaded system normal mode dispersion characteristics is an important aspect of the design phase for any periodic circuit configuration.

The loaded finite length periodic circuit dispersion analysis algorithm is implemented using the frequency dependent mode matching algorithm [2] to create complex vector electromagnetic field maps for the finite length of the periodic circuit shown in Fig. 1. This is accomplished by determining a frequency dependent GSM for each frequency analyzed in a defined frequency span for the entire circuit configuration depicted in Fig. 1. Once the GSM for the entire circuit is determined, then the regional forward and backward wave scattering variable amplitudes are determined for each region of a circuit. Generally, if a circuit is composed of N regions as shown in Fig. 4, then $\vec{a}_1^L$ and $\vec{a}_N^R$ are known, and $\vec{b}_1^L$ and $\vec{b}_N^R$ are determined from the GSM for the given circuit configuration. If the scattering variable amplitudes are required for Region $N-1$, then a GSM is determined for the right (R) and left (L) hand waveguide assemblies shown in Fig. 4. Simple manipulation of the two GSM's yields the Region $N-1$

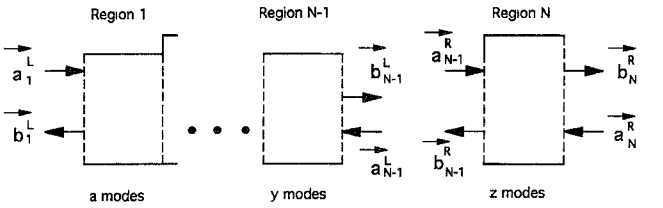

Fig. 4. Arbitrary waveguide representation of a loaded finite length periodic circuit for determining the Region $N-1$ regional normal mode: scattering variable amplitudes.

scattering variables

$$\vec{b}_{N-1}^L = \overline{\overline{S}}_{N-1,1}^L \vec{a}_1^L + \overline{\overline{S}}_{N-1,N-1}^L \vec{a}_{N-1}^L \tag{3}$$

$$\vec{a}_{N-1}^L = (\overline{\overline{1}} - \overline{\overline{S}}_{N-1,N-1}^R \overline{\overline{S}}_{N-1,N-1}^L)^{-1} \overline{\overline{S}}_{N-1,N-1}^R \overline{\overline{S}}_{N-1,1}^L \vec{a}_1^L + (\overline{\overline{1}} - \overline{\overline{S}}_{N-1,N-1}^R \overline{\overline{S}}_{N-1,N-1}^L)^{-1} \overline{\overline{S}}_{N-1,N}^R \vec{a}_N^R. \tag{4}$$

The solution of $\vec{a}_{N-1}^L$ in (4) permits the solution of $\vec{b}_{N-1}^L$ by substituting $\vec{a}_{N-1}^L$ into (3). This procedure determines the scattering variable forward and backward wave amplitudes for Region $N-1$.

This procedure is repeated for the remaining regions of the circuit to determine the unknown scattering variable amplitudes for each region of a finite length periodic circuit. The regional normal mode forward and backward wave scattering variable amplitudes are used to determine the complex electromagnetic field values for any location in the space occupied by the entire waveguide circuit. The complex field values are determined by summing the normal mode expressions as a function of their forward and backward wave amplitudes in each region of the circuit [2], [4], [6]. The appropriate phase shift as a function of location in each region must be included to ensure that the field value being calculated at each location in the waveguide structure is properly represented. The complex field value determined for a point in the periodic circuit represents a point on the field map for the circuit being studied. Field maps for a periodic circuit are created by sequentially determining complex field values for discretized points over the length of the circuit for the direction of propagation through the circuit. The resulting frequency dependent spatial field maps for the length of the periodic circuit are then Fourier analyzed to determine the system normal mode phase and frequency characteristics for the loaded finite length periodic circuit being studied.

Field maps are determined for the length of the periodic circuit for each frequency analyzed. Fourier analysis of each frequency dependent field map yields a given Fourier harmonic spectrum. Each Fourier harmonic corresponds to a given phase shift for the periodic circuit being analyzed by defining the number of periods over which the field maps were created, and knowing the length of each period. The phase associated with each Fourier harmonic is defined as

$$\beta L = \frac{2\pi m}{M}, \qquad m = 0, 1, 2, \cdots, \frac{M}{2} \tag{5}$$

where M is the number of circuit periods over which the field maps were created, and L is the period length in meters. The index m is used to assign a phase to each spatial Fourier

harmonic. The circuit shown in Fig. 1 defines $L = 0.292$ in $= 0.0074$ m, and $M = 8$ for the eight-period circuit. This information is sufficient to create a system normal mode dispersion diagram from the Fourier harmonic information determined by analyzing the frequency dependent field maps created for a loaded periodic circuit.

III. Dispersion Analysis of a Loaded Vane-Type Waveguide Resonator

Conventional TE^z- and TM^z-type modes are capable of propagating on the loaded finite length vane-type waveguide circuit shown in Fig. 1, as well as a host of hybrid modes [2], [3]. In addition, surface wave modes [1], [2] can propagate on the vane-type waveguide circuit forming passband characteristics commonly associated with slow wave circuit applications. The dispersion characteristics for these system normal modes will now be examined by analytically mapping and Fourier analyzing the frequency dependent vector electromagnetic field components for the circuit shown in Fig. 1 using the following regional normal mode expansion for the mode matching algorithm.

The problem geometry shown in Fig. 1 has four regions requiring the definition of a normal mode expansion. These four regions are identified in sequence in Fig. 1 as the WR-90, iris, slot, and vane waveguides where the periodic slot and vane waveguide regions form the periodic circuit. The WR-90 waveguide TE^z regional normal mode indexes include the $m = 0,1,2,3,4,5,6$ and $n = 0,1,2,3$, and the TM^z regional normal mode indexes are $m = 1,2,3,4,5,6$ and $n = 1,2,3$. The iris waveguide TE^z regional normal mode indexes include $m = 0,1$ and $n = 0,1$, and the TM^z regional normal modes indexes are $m = 1$ and $n = 1$. The slot waveguide TE^z regional normal mode indexes are $m = 0,1,2,3,4,5,6$ and $n = 0,1,2,3,4,5,6,7$ modes, while the TM^z regional normal mode indexes include the $m = 1,2,3,4,5$ and $n = 1,2,3,4,5,6,7$ modes. The vane waveguide TE^z regional normal mode indexes include the $m = 0,1,2,3,4,5,6$ and $n = 0,1,2,3,4,5$, modes, and the TM^z regional normal mode indexes are $m = 1,2,3,4,5,6$ and $n = 1,2,3,4,5$. This regional normal mode expansion is sufficient to satisfy the RC criterion for the system normal modes over the 6.5–10.5 GHz frequency span for the first slow-wave mode passband depicted in Fig. 3.

The system normal mode dispersion analysis is performed using discretized E_z field data over the length of the vane-type waveguide resonator periodic circuit shown in Fig. 1 for a frequency span of 6.5–10.5 GHz using 101 frequencies. The E_z field component for the eight-period circuit is discretized using 601 data points at a cross section dimension for the first region of the periodic circuit of $x = 0.443$ in, $y = -0.296$ in. The plotting line is 5 mils below the vane tips, forcing E_z to be approximately zero across the vane tips if the boundary conditions are satisfied with the regional normal mode expansion. The resulting 3-D system normal mode dispersion diagram for the eight-period circuit is shown in Fig. 5, and the corresponding 2-D contour plot dispersion diagram is shown in Fig. 6. The low harmonic amplitude information displayed in Fig. 5 is more clearly displayed

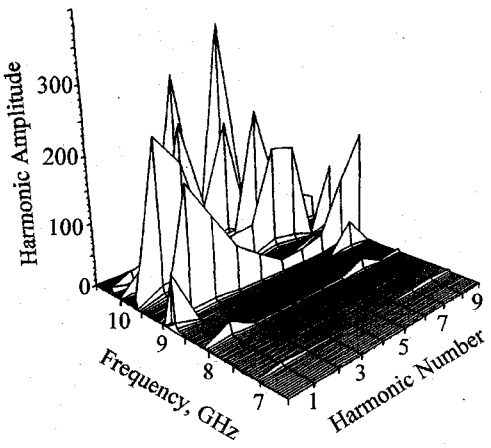

Fig. 5. Three-dimensional system normal mode phase and frequency characteristics for the eight-period loaded finite length linear vane-type waveguide resonator shown in Fig. 1.

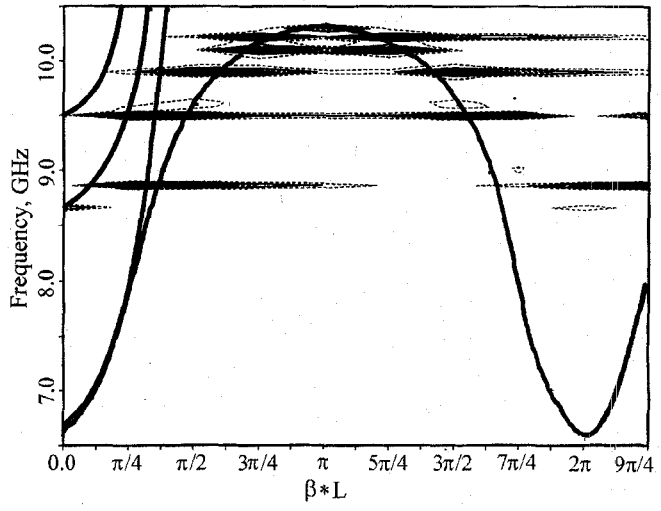

Fig. 6. Two-dimensional system normal mode phase and frequency characteristics for the eight-period loaded finite length linear vane-type waveguide resonator shown in Fig. 1.

as a logarithmic plot shown in Fig. 7. Careful inspection of Figs. 5 and 7 reveals the presence of several transverse ridges for the 3-D dispersion diagram. The GSM dispersion diagram for the infinitely periodic vane-type waveguide shown in Fig. 3 is overlaid on the 2-D contour plot dispersion diagram shown in Fig. 6, where the system normal modes responsible for these transverse ridges are readily identified. This data visualization technique permits the idealized analytic model used to determine the system normal mode phase and frequency characteristics for the infinitely periodic circuit to be directly compared to the information determined by spatially Fourier analyzing the field maps for the finite length periodic circuit.

Inspection of Fig. 3 indicates that there are nine resonances associated with the first slow wave system normal mode passband between 6.5 and 10.5 GHz. The circuit being analyzed is eight periods in length; Fourier analysis of the field maps for these resonances determines the respective amplitudes of the various Fourier harmonics. The $\pi/8$-mode, $3\pi/8$-mode, $5\pi/8$-mode, and $7\pi/8$-mode are defined as odd-order harmonics,

TABLE I
COMPARISON OF THE SYSTEM NORMAL MODE PHASE AND FREQUENCY CHARACTERISTICS ANALYTICALLY DETERMINED USING FIGS 5–7 WITH THE EXPERIMENTAL DATA PRESENTED IN FIG. 3

mode identifier	analytically determined system normal mode resonance frequency determined from Fig. 6	experimentally determined system normal mode resonance frequency determined from Fig. 3	percentage error between Figs. 3 and 6
π-mode	10.300 GHz	10.305 GHz	0.05 %
$7\pi/8$-mode	10.220	10.213	0.07
$3\pi/4$-mode	10.100	10.109	0.09
$5\pi/8$-mode	9.900	9.911	0.1
$\pi/2$-mode	9.620	9.629	0.09
$TM_{1,1,1}$	9.500	9.491	0.09
$3\pi/8$-mode	9.020	9.028	0.09
$EH_{1,1,2}$	8.860	8.853	0.08
$EH_{1,1,1}$	8.660	8.642	0.2
$\pi/4$-mode	8.020	8.018	0.02
$\pi/8$-mode	7.100	7.109	0.1
0-mode	6.660	6.6682	0.1

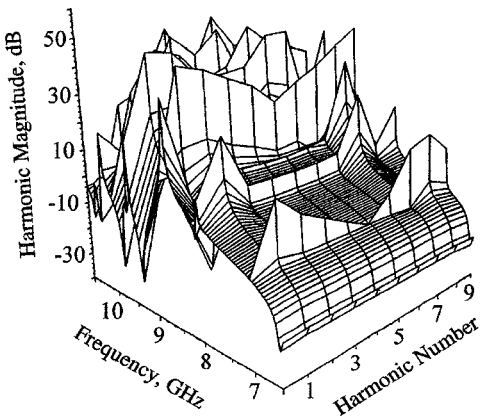

Fig. 7. Logarithmic 3-D system normal mode phase and frequency characteristics for the eight-period loaded finite length linear vane-type waveguide resonator shown in Fig. 1.

while the 0-mode, $\pi/4$-mode, $\pi/2$-mode, $3\pi/4$-mode, and π-mode are defined as even-order harmonics. Fundamentally, the 0-mode corresponds to the excitation of the zeroth Fourier harmonic, the $\pi/4$-mode corresponds to the excitation of the first harmonic, the $\pi/2$-mode corresponds to the excitation of the second harmonic, the $3\pi/4$-mode corresponds to the excitation of the third harmonic, and finally the π-mode corresponds to the excitation of the fourth harmonic. Each mode defined as corresponding to an even-order harmonic is divisible by two, yielding an integer representation of the dominant Fourier harmonic excited by the mode. The modes defined by odd-order harmonics, however, are not divisible by two, which leads to the excitation of asymmetrical Fourier harmonics for these modes. This concept is demonstrated in the following system normal mode analysis.

The system normal mode resonances for the first passband of the periodic circuit dispersion characteristics displayed in Fig. 3 are discussed individually. The resonances are individually field mapped and spatially Fourier analyzed to assist with identifying which system normal modes are being excited with the coupling port geometry depicted in Fig. 1. The analytically determined system normal mode phase and frequency characteristics for each resonance displayed in Fig. 5 are compared in Table I with the experimental dispersion data presented in Fig. 3.

The peak at 10.3 GHz shown in Fig. 6 corresponds to the excitation of the system normal mode π-mode, which corresponds to a zero group velocity for the first passband of the circuit on the dispersion diagram. The field map for this mode is shown in Fig. 8 followed by the Fourier harmonic spectrum in Fig. 9. The π-mode is an even-order harmonic, which leads to the excitation of the fourth Fourier harmonic shown in Fig. 9. The π-mode for this circuit has been experimentally determined to occur at 10.305 GHz, yielding a 0.05% error between the analytical dispersion information presented in Fig. 6 and that obtained experimentally.

It is interesting to note that the π-mode field map shown in Fig. 8 appears to be decaying in amplitude over the length of the circuit. The π-mode occurs at the upper passband cutoff frequency, forcing the slow-wave system normal mode to be cutoff for higher frequencies. Therefore, as the wave is being cutoff or is becoming evanescent, then a longer wavelength component is superimposed on the short wavelength mode. This is illustrated by extending the eight-period circuit to 24 periods in length, where the field map for the 24-period circuit is illustrated in Fig. 10. A long wavelength component is superimposed on the π-mode field map indicating that this is not the exact frequency for the π-mode. The exact frequency for the π-mode will yield an evanescent or decaying field profile for the length of the circuit, demonstrating that the slow-wave mode has achieved the cutoff phenomenon.

The remaining resonances for the first passband of the periodic circuit shown in Fig. 1 have been analyzed using the

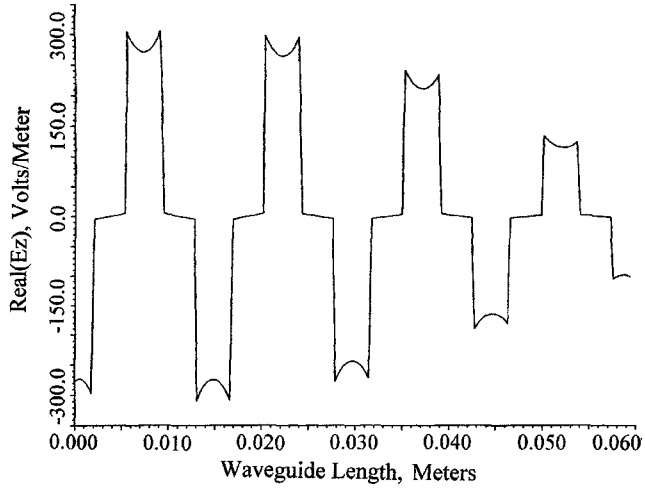

Fig. 8. π-mode $\Re e(E_z)$ field map for the eight-period loaded finite length linear vane-type waveguide resonator shown in Fig. 1.

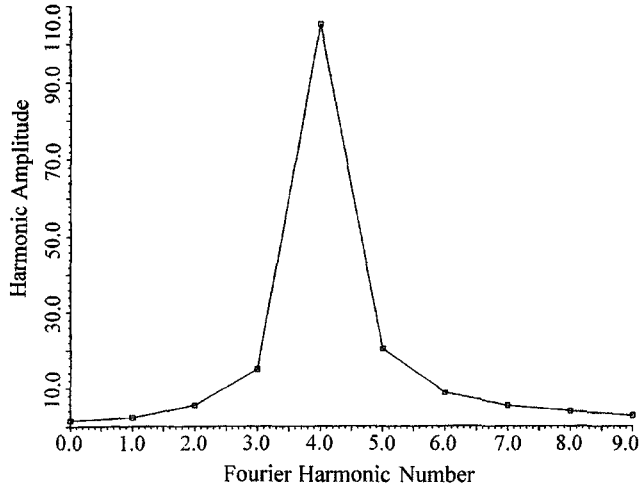

Fig. 9. Fourier harmonic spectrum for the π-mode $\Re e(E_z)$ field map shown in Fig. 8.

E_z field map data and associated Fourier harmonic spectrum demonstrated for the analysis of the π-mode. The results of this analysis are summarized in Table I, which are briefly discussed in the following text.

The next ridge at 10.22 GHz is related to the $7\pi/8$-mode. The $7\pi/8$-mode is an odd order harmonic, leading to the excitation of the third and fifth Fourier harmonics. This ridge is followed by a ridge at 10.1 GHz for the $3\pi/4$-mode. The $3\pi/4$-mode is an even-order harmonic, which leads to the excitation of the third and fifth Fourier harmonics. The $5\pi/8$-mode is an odd-order harmonic occurring at 9.9 GHz, which excites the second and third Fourier harmonics. The ridge at 9.62 GHz is related to the excitation of the $\pi/2$-mode. The $\pi/2$-mode is an even-order harmonic, leading to the excitation of the second and sixth Fourier harmonics.

The following frequency span for the circuit illustrates the ability of the circuit to simultaneously propagate surface wave, hybrid wave, and classical waveguide system normal modes. The two GSM dispersion algorithms are able to analyze this family of mixed mode types. The $TM_{1,1,1}$ mode is excited

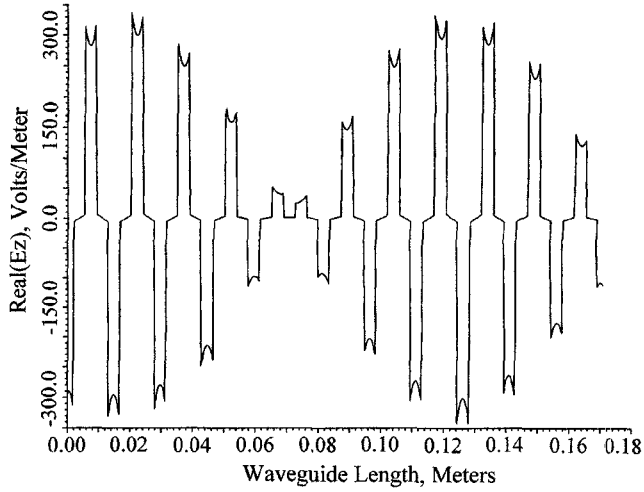

Fig. 10. π-mode $\Re e(E_z)$ field map for a 24-period loaded finite length linear vane-type waveguide resonator.

at 9.5 GHz followed by the $3\pi/8$-mode at 9.02 GHz. The $3\pi/8$-mode is an odd-order harmonic leading to the excitation of the first and second Fourier harmonics. The $EH_{1,1,2}$ mode is excited at 8.86 GHz. Similarly, the ridge at 8.66 GHz is related to the excitation of the $EH_{1,1,1}$ resonator mode with the coupling port geometry. The $EH_{1,1,1}$ and $EH_{1,1,2}$ modes are unique hybrid modes for corrugated waveguide structures.

The ridge at 8.02 GHz is related to the excitation of the $\pi/4$-mode. This region of the dispersion diagram corresponds to the point of divergence for the $TE^{x}_{1,0}$ mode from the slow wave system normal mode associated with the $\pi/4$-mode. The diverging dispersion lines for these two modes can cause passive coupling or energy to be mutually exchanged between the modes, which has been addressed by Johnson [4]. The $\pi/4$-mode is an even order harmonic, leading to the excitation of the first and seventh Fourier harmonics.

The next ridge at 7.1 GHz corresponds to the excitation of the $\pi/8$-mode. The $\pi/8$-mode is an odd-order harmonic, which excites the first and eighth Fourier harmonics. Finally, the transverse valley shown at the bottom of Fig. 7 corresponds to the lower cutoff frequency of the first passband 0-mode shown in Fig. 3. The bandpass cutoff of the 0-mode corresponds to the cutoff frequency of the vane-type waveguide slot mode. The first passband slot mode is comparable to a $TE_{1,0}$ mode propagating in the slots or corrugations forming the resonator, where cutoff is theoretically determined [2], [3], [11] to occur at 6.6682 GHz.

This demonstration using the two analytic methods for determining the system normal mode phase and frequency characteristics of an infinitely periodic circuit, in conjunction with the spatial Fourier analysis algorithm for a finite length periodic circuit, demonstrates the ability of both techniques to produce accurate dispersion information for periodic circuits. These new dispersion analysis techniques form complementary tools. The GSM dispersion algorithm for infinitely periodic circuits [2], [3] determines the classical system normal mode dispersion information, and the spatial field mapping and Fourier analysis algorithm [2] provides a means to explore the excitation of system normal modes with the input and

output port geometries for the circuit under study. The use of both dispersion analysis algorithms provides a method for understanding circuit anomalies causing interference and power loss for specific circuit applications. These two new and powerful dispersion analysis tools are used to resolve a variety of problems associated with the propagation and excitation of various system normal modes for periodic circuits.

IV. Conclusion

This paper has presented a new analytical method for determining the system normal mode dispersion characteristics of a finite length periodic circuit as a function of loading. Vector electromagnetic field mapping techniques were analytically determined using the mode matching algorithm. The resulting field maps were submitted to a spatial Fourier analysis algorithm, where each field map for the circuit was analyzed to determine the spatial Fourier harmonic content. The frequency dependent harmonic information was used to construct a new 3-D and 2-D dispersion diagram for the circuit being analyzed. The new dispersion diagrams present the common frequency and phase information, but also display the amplitude of each harmonic being excited by the coupling port geometry for the periodic circuit.

The resulting dispersion relations for the finite length and the infinitely periodic circuits form complementary analysis tools for the design of loaded periodic circuits. The classical system normal mode dispersion relationship determined from the GSM using Floquet's theorem accurately defines the dispersion characteristics for all of the modes capable of being excited over a designated frequency span. Similarly, the finite length periodic circuit 3-D dispersion diagram and accompanying 2-D contour map dispersion diagram were used to define which system normal modes were being excited and propagated on the finite length periodic circuit by the defined coupling port geometry. Overlaying the infinitely periodic circuit dispersion diagram on the finite length periodic circuit 2-D contour map dispersion diagram permits clear definition of which system normal modes are being excited by the periodic circuit coupling port geometry. Dispersion errors less than 0.2% were demonstrated for a loaded linear vane-type waveguide resonator by comparing dispersion data obtained experimentally with analytical dispersion data obtained using the analytic field mapping and spatial Fourier analysis dispersion algorithm. The modes excited for this circuit included slow wave, hybrid, and classical waveguide system normal modes for the given periodic circuit geometry.

In summary, a new analytic tool has been developed to aid with designing and developing complex periodic structures using the mode matching algorithm. The vane-type waveguide has been the circuit of choice to demonstrate these efficient tools for predicting the system normal mode dispersion characteristics for loaded finite length and infinitely periodic circuits. These new analytic tools offer significant enhancements over historical analysis tools. The new dispersion analysis tools will serve to significantly reduce the design and development time for periodic circuits in industrial or laboratory applications, leading to substantial cost savings using these new design algorithms.

References

[1] R. M. Bevensee, *Electromagnetic Slow Wave Systems*. New York: Wiley, 1964.
[2] W. S. Best, "Dispersion analysis of the loaded vane-type waveguide using the generalized scattering matrix," Ph.D. dissertation, Univ. of Utah, Dept. of Electrical Engineering, Salt Lake City, UT, Mar. 1996.
[3] W. S. Best, R. J. Riegert, and L. C. Goodrich, "Dispersion analysis of the linear vane-type waveguide using the generalized scattering matrix," *IEEE Trans. Microwave Theory Tech.*, vol. 43, no. 9, pp. 2101–2108, Sept. 1995.
[4] C. C. Johnson, *Field and Wave Electrodynamics*. New York: McGraw-Hill, 1965.
[5] W. S. Best and T. A. Treado, "Rotary probe measurements of a crossed-field amplifier slow wave circuit," in *Proc. IEEE Electron Device Society Meet.*, San Francisco, CA, Dec. 1990.
[6] T. Itoh, *Numerical Techniques for Microwave and Millimeter-Wave Passive Structures*. New York: Wiley, 1989.
[7] G. L. James, "Analysis and design of TE_{11}–to–HE_{11} corrugated cylindrical waveguide mode converters," *IEEE Trans. Microwave Theory Tech.*, vol. MTT-29, no. 10, pp. 1059–1066, Oct. 1981.
[8] H. Patzelt and F. Arndt, "Double e-plane steps in rectangular waveguides and their application for transformers, irises, and filters," *IEEE Trans. Microwave Theory Tech.*, vol. MTT-30, no. 5, pp. 771–776, May 1982.
[9] R. Mittra, T. Itoh, and T.-S. Li, "Analytical and numerical studies of the relative convergence phenomenon arising in the solution of an integral equation by the moment method," *IEEE Trans. Microwave Theory Tech.*, vol. MTT-20, no. 2, pp. 96–104, Feb. 1972.
[10] R. Mittra and S. W. Lee, *Analytical Techniques in the Theory of Guided Waves*. New York: Macmillan, 1971.
[11] D. R. Gunderson and R. W. Grow, "A theoretical and experimental investigation of the feasibility of constructing high power two-millimeter backward-wave oscillators using ladder and vane-type slow-wave structures," Tech. Rep. AFAL-TR-69-259, Air Force Avionics Laboratory, Air Force Systems Command, Wright-Patterson Air Force Base, OH, Oct. 1969.

W. Scott Best (S'79–M'80), for photograph and biography, see p. 2108 of the September 1995 issue of this Transactions.

Ronald J. Riegert, for photograph and biography, see p. 2108 of the September 1995 issue of this Transactions.

Lewis C. Goodrich, for photograph and biography, see p. 2108 of the September 1995 issue of this Transactions.